JOURNAL OF SOLID STATE CHEMISTRY 110, 216–225 (1994)

Phase Relationship and Lithium Deintercalation in Lithium Nickel Oxides

R. Kanno,[1] H. Kubo, and Y. Kawamoto

Department of Chemistry, Faculty of Science, Kobe University, Kobe, Hyogo, 657 Japan

T. Kamiyama

Institute of Materials Science, University of Tsukuba, Tsukuba, Ibaraki, 305 Japan

F. Izumi

National Institute for Research in Inorganic Materials, Tsukuba, Ibaraki, 305 Japan

Y. Takeda

Department of Chemistry, Faculty of Engineering, Mie University, Tsu, Mie, 514 Japan

and

M. Takano

Institute for Chemical Research, Kyoto University, Uji, Kyoto, 611 Japan

Received June 9, 1993; in revised form August 31, 1993; accepted September 1, 1993

The phase relationship between $LiNiO_2$ and its related compounds was examined by X-ray diffraction, neutron diffraction, DTA-TG, and electrical, magnetic, and electrochemical measurements. Decomposition of $LiNiO_2$ proceeded at higher temperatures to $Li_{1-x}Ni_{1+x}O_2$ with the partially disordered α-$NaFeO_2$ structure and $Li_xNi_{1-x}O$ with the fully disordered rock-salt structure. Higher oxygen partial pressure in the atmosphere suppressed the decomposition reaction, which was considered to be the reduction from Ni^{3+} to Ni^{2+} state. The nearly stoichiometric "$LiNiO_2$" was synthesized at reaction temperatures below 700°C in an oxygen gas flow with the starting materials Li_2O_2 and NiO. Neutron diffraction measurement confirmed the composition $Li_{0.996}Ni_{1.006}O_2$, which is very close to the stoichiometry. The deintercalation mechanism of $LiNiO_2$ and the spinel transformation process from $Li_{1-x}NiO_2$ to $Li_yNi_2O_4$ were examined; the deintercalation proceeded from $LiNiO_2$ to $Li_{0.3}NiO_2$ monophasically when the cell configuration allowed a homogeneous reaction. The range of solid solutions $0.8 \le y \le 1.8$ was observed for the spinel $Li_yNi_2O_4$ transformed from $Li_{1-x}NiO_2$ ($0.1 \le x \le 0.6$) by heat treatment at 180°C. The room-temperature intercalation to the spinel $LiNi_2O_4$ gave the new polymorphism $Li_2Ni_2O_4$ ($LiNiO_2$) with the cubic lattice parameter a = 8.207(3) Å. Electrical properties of the spinels were also examined. © 1994 Academic Press, Inc.

[1] To whom correspondence should be addressed.

INTRODUCTION

The layered nickel oxides $LiNiO_2$ have been studied for possible use as insertion electrodes in 4V rechargeable lithium batteries (1–3). In $LiNiO_2$, alternate layers of Li and Ni occupy the octahedral sites of a cubic close packing of oxide ions, making up a rhombohedral structure with an $R\bar{3}m$ space group, Li in 3*a*, Ni in 3*b*, and O in 6*c* sites. This compound shows structural and compositional varieties depending on their synthesis conditions. Figure 1 shows the phase relationship between $LiNiO_2$ and its related compounds reported previously, together with the results obtained in the present study. Only the Li NiO_2–NiO solid solution could be synthesized at elevated temperatures. Other phases, such as $Li_{1-x}NiO_2$, Li_2NiO_2, and $LiNi_2O_4$, were obtained by room-temperature intercalation or by low-temperature (<300°C) heat treatment. The results reported previously are as follows.

(i) The stoichiometric $LiNiO_2$ is difficult to obtain, because the high-temperature treatment of $LiNiO_2$ leads to a decomposition from $LiNiO_2$ to $Li_{1-x}Ni_{1+x}O_2$, which has a partially disordered cation distribution at the Li site (4, 5). The stoichiometry of $LiNiO_2$ affects the physical properties; the nonstoichiometry led to a significant degradation in the charge and discharge characteristics (6) and

0022-4596/94 $6.00
Copyright © 1994 by Academic Press, Inc.
All rights of reproduction in any form reserved.

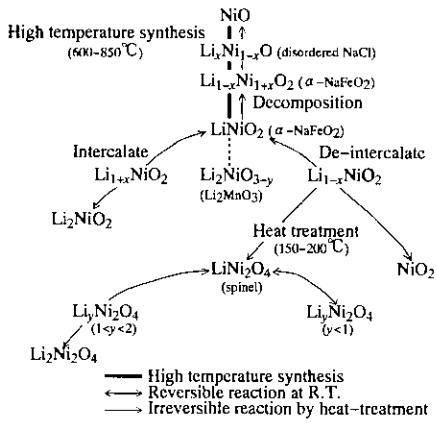

FIG. 1. Phase relationship for $LiNiO_2$ and related compounds.

the magnetic properties were extremely sensitive to its cation distribution (7, 8).

(ii) Room-temperature intercalation and deintercalation give a certain range of solid solution, $Li_{1-x}NiO_2$ ($-1.0 \leq x \leq 0.7$). The electrochemical deintercalation of $Li_{1-x}NiO_2$ ($0 \leq x \leq 0.7$) reported by Thomas *et al.* proceeded from x = 0.0 (3.5 V) to 0.6 (4.2 V) with two plateaus in the OCV curve around $x = 0.33$ and 0.45, which were attributed to a Li-vacancy ordering within the Li plane (1). In contrast, Dahn *et al.* indicated no plateaus on the cell-voltage vs composition x curve (2); their *in situ* X-ray diffraction measurements of $Li_{1-x}NiO_2$ ($0 \leq x \leq 0.6$) showed a monophasic reaction. Lithium intercalation was reported for $Li_{1-x}NiO_2$ ($-1.0 \leq x \leq 0.0$). The structure of the end-member, Li_2NiO_2, determined by the neutron diffraction measurement was composed of an hcp oxide ion array in which lithium and nickel ions occupy the octahedral sites in an ordered manner (2, 9).

(iii) The deintercalated $Li_{0.5}NiO_2$ with the α-$NaFeO_2$ structure transforms to the spinel structure by low-temperature heat treatment (1). The transformation proceeded above 150°C and the spinel decomposed above 300°C. The electrical and magnetic properties were reported for the spinel $LiNi_2O_4$ (10). However, a formation of solid solutions has not been reported.

Attempts to synthesize the stoichiometric $LiNiO_2$ have been made by changing Li to Ni ratios, heating temperatures, or starting materials such as lithium peroxide (1), lithium hydrate (11), and lithium nitrates (6). However, in order to synthesize the stoichiometric $LiNiO_2$, the decomposition process at higher temperatures should be clarified. In the present study, we first precisely examined the decomposition process from $LiNiO_2$ to $Li_{1-x}Ni_{1+x}O_2$ at higher temperatures. We synthesized "$LiNiO_2$" which is very close to the stoichiometric composition; its structure was determined by neutron diffraction measurement. The relationship among the compositions, the structures, and the physical properties is discussed. Second, we reexamined the deintercalation process of $Li_{1-x}NiO_2$ using electrochemical cells with different cell constructions. Third, the transformation process from the α-$NaFeO_2$ to the spinel structures was studied with varying heating temperature and time for $Li_{1-x}NiO_2$ with $0 < x \leq 0.6$. Further, the electrochemical characteristics of the spinel were examined.

EXPERIMENTAL

The ternary oxide $LiNiO_2$ was prepared by heating appropriate molar ratios of Li_2O_2 and NiO (Li_2O_2: Alfa. Ltd., >95.3% purity; NiO: Nakarai tesk, >99.9% purity). They were mixed, pelletized in an argon filled glove box, and then heated in the range 450–850°C. Reactions were carried out under oxygen gas flow, under nitrogen gas flow, or in air.

X-ray diffraction patterns of the powdered samples were obtained with an X-ray diffractometer (Rigaku RAD-C) with Cu$K\alpha$ radiation. The diffraction data were collected for 10 sec at each 0.02° step over a 2θ range from 10 to 100°. The lattice parameters of the lithium nickel oxides, $Li_{1-x}Ni_{1+x}O_2$, were refined by Rietveld analysis using the computer program RIETAN (12). Reflection positions and intensities were calculated for both Cu$K\alpha_1$ and Cu$K\alpha_2$ with a factor of 0.5 applied to the latter's calculated integrated intensities. A pseudo-Voigt profile function was used; the mixing parameter γ was included in the least-squares refinements.

The samples after the electrochemical test were mounted on a specially designed X-ray holder in an argon atmosphere. A 7-μm-thick aluminum window covered the sample holder to prevent moisture attack during the measurement. Lattice parameters were calculated against an internal silicon standard.

Neutron diffraction data were taken on a time-of-flight (TOF) neutron powder diffractometer, HRP (13), at the KENS pulsed spallation neutron source at the National Laboratory for High Energy Physics (KEK). The specimen was contained in a cylindrical vanadium cell 5 mm in radius, 55 mm in height, and 200 μm in thickness. The average scattering angle, 2θ, was fixed at 170°, and intensity data were collected at 300 K.

The electrochemical intercalation and deintercalation were carried out using lithium cells. Two types of cells with different working electrodes were used. The working electrode of cell (I) consisted of a mixture of 50 mg $LiNiO_2$, 5 mg acetylene black, and 5 mg Teflon powder pressed into a tablet of 13 mm diameter under a pressure of 9 MPa. The working electrode of cell (II) consisted of 50 mg $LiNiO_2$ pressed under a pressure of 9 MPa. The cells used for the electrochemical tests were constructed

in a cylindrical configuration described previously (14) or in a stainless steel 2016 coin-type configuration (20 mm outside diameter and 1.6 mm thickness). The counter electrode was a 15-mm-diameter and 0.24-mm-thickness disk of lithium metal foil. The separator employed was a microporous polypropylene sheet. Typical electrolytes used in these cells were 1 M solutions of $LiClO_4$ in a 50 : 50 mixture of propylene carbonate (PC) and 1,2-dimethoxyethane (DME) (Mitsubishi Petrochemical Company Ltd., battery grade) by volume. All reagents were dried in a standard manner (15, 16). The water content of the electrolytes was less than 20 ppm. The cells were constructed in an argon filled glove box.

The current density was calculated based on the cathode area. The electrochemical measurements were carried out at room temperature after standing overnight under zero current flow. Cell properties were measured galvanostatically. Quasi-open-circuit voltages (OCV) were measured by alternating discharge and rest periods. A constant current of 0.1 mA/cm^2 was passed through the cell for some period, and the cell voltages on an open circuit were considered as the quasi-OCV when the change in the measured cell voltage was less than 1 mV. After the electrochemical test, the $LiNiO_2$ electrodes were used for X-ray diffraction measurements and heat treatment experiments without washing or drying.

The electrical resistivity was measured for the sintered materials with dimensions of approximately 2 × 2 × 5 mm. The data were obtained by the dc four-probe method in the temperature range $15 \leq T \leq 300$ K using a Toyo-sanso low-temperature electrical-conductivity measurement unit. The reaction and weight loss of the lithium nickel oxides upon being heated to 1000°C were measured by an automatic differential thermal analysis-thermogravimetry (DTA-TG) apparatus of Rigaku TAS-100. Magnetic susceptibility was measured by a SQUID magnetometer (Quantum Design, MPMS2) at between 5 and 300 K in a field of 1 kG. The sign and magnitude of the applied magnetic field were determined with granular Pb metal.

RESULTS AND DISCUSSION

(a) $LiNiO_2$

Synthesis

We synthesized the samples according to the method of Thomas *et al.* (1). The reactions in an oxygen gas flow at 650–850°C for 48 hr gave rhombohedral $LiNiO_2$; only a mixture of Li_2NiO_{3-y} (17) and NiO was obtained below 500°C. Table 1 summarizes the X-ray Rietveld refinement results for $LiNiO_2$ synthesized at 650–850°C. The lattice parameters of the reaction products increase slightly from $a = 2.87584(6)$ and $c = 14.1905(4)$ Å at 650°C to $a = 2.87899(5)$ and $c = 14.1922(4)$ Å at 850°C. Li *et al.* reported that the lattice parameters of the solid solution, $Li_{1-x}Ni_{1+x}O_2$, increased with x, or in proportion to the disordering of the cation distribution (5). The increase in the lattice parameters with reaction temperature indicates a decomposition of $LiNiO_2$ to $Li_{1-x}Ni_{1+x}O_2$ at higher temperatures (2). The compositions determined by atomic absorption spectroscopy were $Li_{0.99}Ni_{1.01}O_2$ ($Ni^{2.98+}$), $Li_{1.00}Ni_{1.00}O_2$ ($Ni^{3.00+}$), and $Li_{0.93}Ni_{1.07}O_2$ ($Ni^{2.87+}$) for the samples synthesized at 650, 700, and 850°C, respectively. Synthesizing temperatures below 700°C led to the nearly stoichiometric "$LiNiO_2$."

Phase Relation at Higher Temperatures

Figure 2 shows the TG curves for the samples synthesized at 850°C. The TG curve in an oxygen gas flow showed a slight weight gain at around 800°C, and afterward showed a large decrease in weight at around 920°C accompanied by an endothermic DTA peak. The X-ray diffraction pattern of the sample after the DTA-TG measurement was indexed by a cubic cell of $a = 4.1231(15)$ Å, indicating a decomposition of $LiNiO_2$ to $Li_xNi_{1-x}O$. The decomposition temperature shifted from 750 to 920°C with increasing oxygen partial pressure in the measurement atmosphere.

To understand the reaction mechanism at higher temperatures, we examined the decomposition process by annealing samples in air or in an oxygen gas flow at various temperatures. The samples synthesized at 850°C were annealed at 300, 450, 600, 700, 850, and 1000°C in air or in an oxygen gas flow and then quenched in liquid N_2. The X-ray diffraction pattern of the sample annealed at 1000°C was different from those of the samples annealed below 700°C. The structural parameters of these samples were refined using the structural models as follows: the cubic $Li_xNi_{1-x}O$ with disordering cation distribution (space group $Fm3m$) for the 1000°C sample; the rhombo-

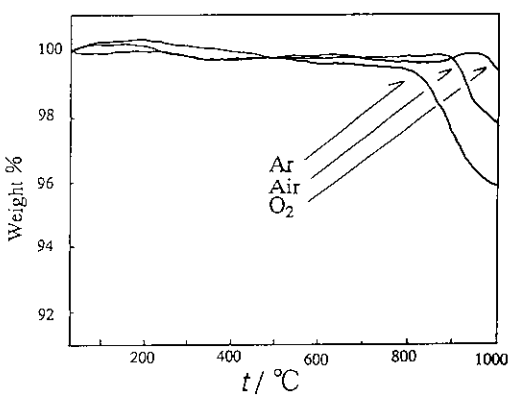

FIG. 2. TG curves for $LiNiO_2$ synthesized at 850°C in O_2 atmosphere.

TABLE 1
X-Ray Rietveld Refinement Results for the Lithium Nickel Oxides

Sample/ Condition	R_{wp}	R_I	a (Å)	c (Å)	g^a	z(O)
			Synthesis			
650°C oxygen	15.09	2.13	2.87584(6)	14.1905(4)	0.976(13)[b]	0.2412(13)
700°C oxygen	16.51	2.30	2.87642(6)	14.1913(4)	0.978(14)[b]	0.2408(13)
850°C oxygen	15.15	2.88	2.87899(5)	14.1922(3)	0.970(13)[b]	0.2405(14)
700°C $p(O_2)$ = 150 atm	17.06	3.50	2.87442(8)	14.1873(5)	0.972(2)[b]	0.2420(19)
800°C $p(O_2)$ = 150 atm	16.58	3.42	2.87542(5)	14.1850(3)	0.982(19)[b]	0.2428(18)
			Annealing			
300°C air	12.28	1.68	2.88165(4)	14.2004(3)	0.942(13)[b]	0.2417(16)
450°C air	14.84	2.64	2.88328(5)	14.2003(3)	0.919(17)[b]	0.243(2)
600°C air	13.80	2.40	2.88191(5)	14.1959(3)	0.915(15)[b]	0.2422(19)
700°C air	19.45	4.22	2.88668(8)	14.2038(6)	0.87(2)[b]	0.242(3)
850°C air	11.24[c]	10.17	2.8950(2)	14.221(2)	1.0	0.232(7)
		3.69	4.11027(9)[d]			
1000°C air	14.91	7.40	4.1438(1)[d]			
450°C oxygen	14.50	2.60	2.88037(7)	14.1937(5)	0.955(19)[b]	0.2403(18)
600°C oxygen	14.32	2.37	2.87939(6)	14.1912(4)	0.961(17)[b]	0.2403(17)
850°C oxygen	21.16	5.12	2.88348(7)	14.1989(5)	0.92(2)[b]	0.238(2)
			Deintercalation			
$Li_{0.65}NiO_2$	17.92	7.21	2.85199(18)	14.3107(15)	0.65	0.232(2)
$Li_{0.4}NiO_2$	19.27	5.30	2.84790(13)	14.3327(11)	0.40	0.234(2)

[a] Occupancy of Li at the 3*a* site. The occupation factor of Ni at the 3*b* site was fixed at unity.
[b] The occupation factor of Li was refined using the constraint that a total occupancy of Li and Ni at the 3*a* site was unity.
[c] Refinement based on a mixture of $R\bar{3}m$ and $Fm3m$ phases.
[d] The lattice parameter of the cubic $Fm3m$ phase with the disordered NaCl structure.

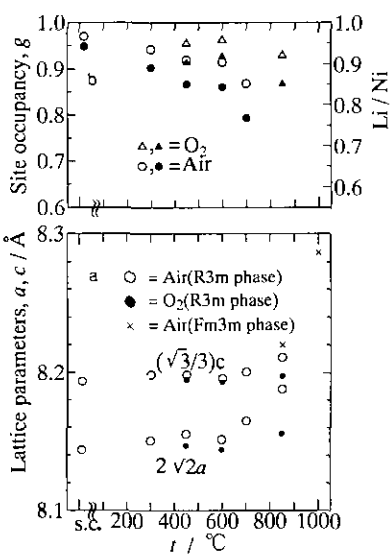

FIG. 3. (a) Annealing temperature dependence of the lattice parameters in $LiNiO_2$. (b) Annealing temperature dependence of the lithium occupancy rate in the Li site, and Li/Ni ratio; g values for the samples annealed in O_2 (△) and in air (○); Li/Ni ratios for the samples annealed in O_2 (▲) and in air (●). S.C. indicates the samples cooled slowly from 850°C in O_2 atmosphere.

hedral $Li_{1-x}Ni_{1+x}O_2$ with partial disordering at the Li site (space group $R\bar{3}m$) for the samples below 700°C; and a mixture of the cubic $Fm3m$ and the rhombohedral $R\bar{3}m$ phases for the 850°C sample. Table 1 lists the refinement results. Figure 3a shows the annealing temperature dependence of the lattice parameters for "$LiNiO_2$." The lattice parameters of the rhombohedral $R3m$ phase increase with annealing temperature from 600 to 850°C in air. The rhombohedral phase decomposed to the cubic $Fm3m$ phase above 850°C. The lithium occupancy rate at the Li site, shown in Fig. 3b, also decreases with annealing temperature. On the other hand, only a slight increase in the rhombohedral (hexagonal) lattice parameters and no decomposition to the cubic phase were observed for the samples annealed below 850°C in an oxygen gas flow, which is consistent with our TG results that the decomposition temperature shifted to higher temperatures with increasing partial oxygen pressure in the measurement atmosphere. The oxidizing condition suppressed the decomposition of $LiNiO_2$ and the reduction from Ni^{3+} to Ni^{2+} state. We tried to synthesize the stoichiometric samples under a high oxygen pressure using the test tube method. The starting materials, Li_2O_2 and NiO, were

TABLE 2
Structural Parameters for $LiNiO_2$ in $R\bar{3}m$ (T = 300 K)

Atom	Site	g	x	y	z	B (Å^2)	
Li	3*a*	0.996(5)[a]	0	0	0	1.6(2)	
Ni(1)	3*a*	0.004	0	0	0	$=B$(Li)	
Ni(2)	3*b*	1.0	0	0	½	0.31(2)	
Ni(3)	6*c*	0.002(2)	0	0	0.131	$=B$(Ni(2))	
O	6*c*	1.0	0	0	0.24111(16)	0.86[b]	
Atom	U_{11}(Å^2)[c]	U_{22}(Å^2)	U_{33}(Å^2)		U_{12}(Å^2)	U_{13}(Å^2)	U_{23}(Å^2)
O	0.0110(6)	$= U_{11}$	0.0070(6)		$= U_{11}/2$	0	0

Note. a = 2.87799(8) Å, c = 14.1953(3) Å, R_{wp} = 3.65%, R_p = 2.82%, R_I = 2.64%, R_F = 1.65%, $S = R_{wp}/R_e$ = 1.17.

[a] Numbers in parentheses are estimated standard deviations of the last significant digit, and those without deviations were fixed under the constraint that the total occupancy of 3*a* site is unity.

[b] Equivalent isotropic thermal parameters, B_{eq}.

[c] The form of the anisotropic temperature factor is $\exp[-2\pi^2(h^2a^{*2}U_{11} + k^2b^{*2}U_{22} + l^2c^{*2}U_{33} + 2hka^*b^*U_{12} + 2hla^*c^*U_{13} + 2klb^*c^*U_{23})]$.

mixed, pelletized, and heated under 100–150 atm oxygen pressure. The X-ray Rietveld refinement results are summarized in Table 1. The samples synthesized under oxygen pressure showed slightly smaller lattice parameters. However, no significant difference in occupancies was found between the samples synthesized at 1 and 150 atm, as shown in Table 1.

Neutron Diffraction Measurements

Neutron diffraction data were obtained for the sample synthesized at 700°C in an oxygen gas flow. Intensity data for interplanar spacings between 0.5 and 2.5 Å were used for Rietveld analysis, but those in TOF regions 12450–12700 and 14650–14850 μsec were excluded in the refinement owing to the appearance of very weak peaks due to Li_2CO_3. The structure was therefore refined with space group $R\bar{3}m$ with the structural model Li at 3*a* (0, 0, 0), Ni at 3*b* (0, 0, ½), O at 6*c* (0, 0, *z*) with $z \approx 0.25$. The partial disordering of Li and Ni at the Li(3*a*) and Ni(3*b*) sites was considered with the constraint that the total occupancy at each site be unity. The site occupation parameters g were refined together with isotropic thermal parameters B. Since the g value of Li in the Ni(3*b*) site became negative, the g value of Ni at this site was fixed at unity. The $|F_{obs}|$ Fourier map showed positive nuclear densities at the tetrahedral site near the Ni(3*b*) site. Then the occupancy of Ni at this tetrahedral site, 6*c* (0, 0, *z*), was refined using the constraint that its B value be equal to that of the Ni(3*b*) site and its z value be fixed at a value obtained from the Fourier $|F_{obs}|$ map. In the final refinement cycle, an anisotropic temperature factor was assigned for the oxygen site. No preferred orientation was corrected. Table 2 lists final R factors (12), lattice and structural parameters, and their estimated standard deviations. Table 3 gives interatomic distances calculated with ORFFE (18). Figure 4 illustrates the profile fit and difference patterns for $LiNiO_2$. The solid lines are calculated

TABLE 3
Interatomic Distances in $Li_{1-x}NiO_2$ in Å

	$LiNiO_2$ at 700°C			
	Neutron	X-ray	$Li_{0.65}NiO_2$	$Li_{0.4}NiO_2$
Li(1)–O	2.1154(14)	2.116(12)	2.19(2)	2.17(2)
Ni(1)–O	1.9692(12)	1.966(11)	1.90(2)	1.91(2)
Ni(2)–Ni(2)	2.8780			
Li–Ni(2)	2.8911			

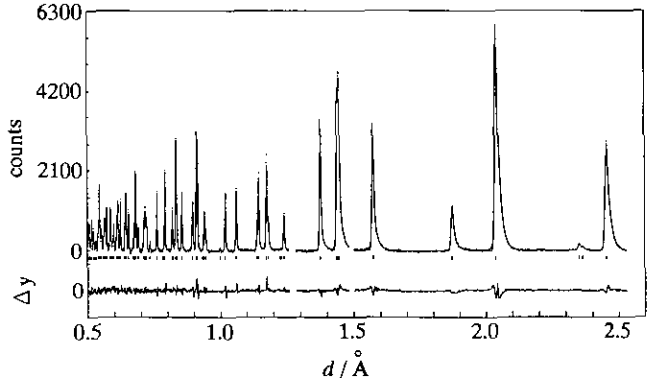

FIG. 4. Observed, calculated, and difference plots for $LiNiO_2$ synthesized at 700°C.

intensities, dots overlying them are observed intensities, and Δy_i is the difference between observed and calculated intensities. Figure 4 shows that the calculated pattern fits the observed one fairly well. Table 3 summarizes the interatomic distances calculated from both the neutron and X-ray diffraction data.

The best fit between observed and calculated data in $LiNiO_2$ synthesized at 700°C yielded the α-$NaFeO_2$ structure in which the 3*a* and 3*b* octahedral sites were mainly occupied by lithium and nickel ions, respectively. The lithium occupancy at the Li site was determined to be 0.996(5), indicating that the sample was nearly stoichiometric. The interstitial tetrahedral site Ni(3) at a position $(0, 0, \frac{1}{8})$ is situated in the NiO_6 octahedral layers. Attempts to refine the occupancy of this site led to an insignificant site occupancy of 0.002(2). Gummow *et al.* (19) have also refined the cobalt occupancy on the tetrahedral 6*c* site in $LiCoO_2$ synthesized at 400°C, and obtained an insignificant occupancy, corresponding to our results on $LiNiO_2$. Finally, the refined composition $Li_{0.996}Ni_{1.006}O_2$ is in excellent agreement with the expected $LiNiO_2$ stoichiometry.

A neutron diffraction study has been reported for a lithium nickel oxide synthesized at 800°C in air for 3 hr (20). Its composition was determined to be $(Li_{0.87}Ni_{0.13})_{3a}[Li_{0.03}Ni_{0.97}]_{3b}O_2(Li_{0.9}Ni_{1.1}O_2)$, and the interatomic distances were 2.1159 Å for Li–O and 1.9793 Å for Ni–O distances. The structures of $Li_{1-x}Ni_{1+x}O_2$ have also been reported for $0.2 \leq x \leq 0.36$ (21). The interatomic distances are in the range of 1.9860–2.0094 Å for Ni–O distances and 2.1015–2.1106 Å for Li–O distances. Figure 5 shows the composition dependence of the interatomic distances in $Li_{1-x}Ni_{1+x}O_2$. The Li–O distances decrease and the Ni–O distances increase with x. These changes can be explained in terms of the difference in ionic radii, r, for octahedral coordination (Ni^{3+}[low spin]: $r = 0.60$ Å; Ni^{2+}: $r = 0.70$ Å; Li^+: $r = 0.74$ Å). The lithium ions at the Li site are replaced by smaller Ni^{3+} ions with an occupancy of x, and the Ni^{3+} ions in the Ni site are reduced to Ni^{2+} ions with larger ionic radii; the cation disordering on the octahedral site leads to shorter Li–O and longer Ni–O distances. Quite recently, neutron diffraction data have been reported for $LiNiO_2$ synthesized from $LiOH \cdot H_2O$ and NiO (11). The sample was synthesized at 650°C in an atmosphere with a dew point of 0°C followed by two preheating processes at 650°C in moisture-free and CO_2-free air. Its composition was determined to be $Li_{0.98}Ni_{1.02}O_2$, and was very close to the $LiNiO_2$ stoichiometry. The bond lengths calculated from the data of Reimers *et al.* (11) are 1.964 Å (Ni–O) and 2.115 Å (Li–O), which are consistent with our data.

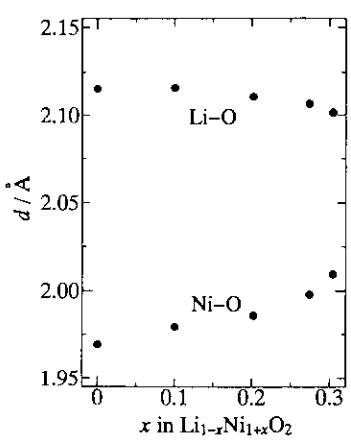

FIG. 5. Composition dependence of the bond distances for $Li_{1-x}Ni_{1+x}O_2$. Data for $x = 0.1$, 0.2, 0.27, and 0.32 are taken from Refs. (20, 21).

Electrical and Magnetic Properties

Magnetic susceptibility was measured in the present study for the samples synthesized at 700 and 850°C in an oxygen gas flow. The sample synthesized at 700°C showed spin glass behavior in the form of irreversibilities below the freezing temperature $T_f \approx 10$ K, and a cusp in the zero field cooling susceptibility. However, no cusp was observed for the sample synthesized at 850°C. These results are consistent with the recent magnetic data reported by Reimers *et al.* (11). The electrical resistivity was measured for $LiNiO_2$ synthesized at 700 and 850°C. Both samples showed semiconducting behavior with the activation energy of around 0.2 eV. The resistivity value of 3×10^1 Ω cm at room temperature for the sample synthesized at 850°C is almost the same as that reported previously (10). However, the sample synthesized at 700°C showed a room-temperature resistivity of 1.0 Ω cm, which is slightly smaller than that of the sample synthesized at 850°C. Further study based on structure analysis and magnetic and electrical measurements is necessary to elucidate the conduction mechanism.

Electrochemical Characteristics

De-intercalation. Our deintercalation experiments using $LiNiO_2$ synthesized at 850°C with the cell(I) showed a monophasic reaction from $x = 0.0$ to 0.7. Figure 6a shows the quasi-OCV curve for $Li_{1-x}NiO_2$. No plateau was observed in the curve. However, changes in slope were observed around $x = 0.3$–0.4 and 0.5–0.6, where the plateaus were indicated by Thomas *et al.* (1). Figure 6b shows the lattice parameter change with composition x. The a-axis decreases and the c-axis increases with increasing x in $Li_{1-x}NiO_2$. These changes are almost the same as those reported previously (1, 7).

In the present study, we tried to make the deintercalated samples without Teflon binder and acetylene black conducting component, because the samples might react with

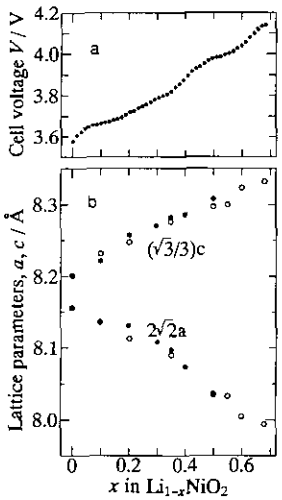

FIG. 6. (a) Quasi-OCV curve for $Li_{1-x}NiO_2$ measured by the cell(I). (b) Lattice parameters vs composition curves for $Li_{1-x}NiO_2$. These data were measured by ●: cell(I), and ○: cell(II).

these impurities during the heat treatment process for spinel transformation. The deintercalation experiments were therefore carried out using the cell(II). The X-ray diffraction patterns for the samples measured just after the deintercalation experiments indicated monophasic properties in the narrow composition regions around $x = 0$, $x = 0.33$, and $x = 0.4$, and the mixtures of two $LiNiO_2$-related phases with different lattice parameters. However, the X-ray diffraction patterns for the samples after the electrochemical experiments changed with a rest period; lithium ionic diffusion at room temperature is high enough to enlarge the monophasic regions. The diffraction data which were taken after 2 weeks of standing followed by the electrochemical deintercalations indicated monophasic properties for the composition ranges $0.0 \leq x \leq 0.2$, $0.35 \leq x \leq 0.4$, and $x \geq 0.5$.

In summary, the deintercalation experiments of $Li_{1-x}NiO_2$ showed the monophasic reaction from $x = 0.0$ to 0.7, consistent with the results of Dahn *et al.* (2). However, when we used the cathodes without acetylene black and Teflon binder, the deintercalation did not proceed by a homogeneous reaction. The X-ray diffraction patterns after 2 weeks of standing followed by the electrochemical deintercalations indicated monophasic properties for the composition ranges $0.0 \leq x \leq 0.2$, $0.35 \leq x \leq 0.4$, and $x \geq 0.5$; the two-phasic regions $0.2 < x < 0.35$ and $0.4 < x < 0.5$ correspond respectively to the plateau regions near $x \approx 0.3$ and 0.45 reported by Thomas *et al.* (1). The difference in reaction mechanism with the cell configurations suggests that the deintercalation mechanism changes with charge–discharge current density.

The structures were refined by the X-ray Rietveld method for the monophasic samples of deintercalated $Li_{1-x}NiO_2$ with $x = 0.35$ and 0.6 ($Li_{0.65}NiO_2$ and $Li_{0.4}NiO_2$). Table 1 summarizes the refinement results. The interatomic distances are listed in Table 3. The Li–O distance increases from 2.1154 Å ($x = 0.0$) to 2.17–2.19 Å ($x = 0.35$ and 0.60), and the Ni–O distance decreases from 1.9692 Å ($x = 0.0$) to 1.90–1.91 Å ($x = 0.4$ and 0.65). These changes are explained by the introduction of vacancy at the Li site, which leads to longer Li–O distances. On the other hand, the oxidation from Ni^{3+} to Ni^{4+} leads to shorter Ni–O distances. Similar results have been reported for $LiCoO_2$; the neutron diffraction measurements revealed that the Li–O distance increased from 2.08 Å at $x = 0.0$ to 2.10 Å at $x = 0.6$, and the Co–O distance decreased from 1.945 Å at $x = 0.0$ to 1.904 Å at $x = 0.6$ Å. The cobalt migration was also observed from the Co plane to the delithiated Li plane. For $LiVO_2$, the deintercalation proceeded by alternating monophasic and biphasic reactions. The single-phase region of $(1 - x) \leq 0.33$ in $Li_{1-x}VO_2$ is stabilized by an ordered arrangement of one-third of the V atoms in the planes that were originally all Li atoms (22, 23). Similar migration might be possible for the lithium nickel oxide. Further study on neutron diffraction for the delithiated $LiNiO_2$ is necessary.

Reversibility. The reversibility of the lithium cell, $Li/LiNiO_2$, was examined using $LiNiO_2$ prepared at 650, 700, and 850°C. The current density was 0.75 mA/cm^2 and the cutoff voltages were 2.5 V for discharge and 4.3 V for charge, respectively. The samples used for the electrochemical test were handled under argon atmosphere in order to avoid the decomposition of Li_2O to lithium hydrate, which might be formed in the grain boundary. Figure 7 shows charge–discharge curves for lithium cells with $LiNiO_2$ synthesized at different temperatures. Excellent reversibility was observed for the cells with the cathodes prepared at 650 and 700°C with a specific capacity of about 150 mAh/g. However, a lower capacity of about 130 mAh/g and a poor reversibility were observed for the cathode prepared at 850°C. The cation disordering on the octahedral sites affects the reversibility as indicated by the previous studies (5, 6).

(b) $Li_yNi_2O_4$

Spinel Transformation

We examined the transformation condition of $Li_{0.5}NiO_2$ with varying temperature from 150 to 300°C and annealing time from 24 to 336 hr. Figure 8a shows the annealing-time dependence of lattice parameters for the samples annealed at 180°C. After 96 hr of annealing, a new peak appeared around 25°, which could be indexed as 220 of a cubic cell of $a = 8.087$ Å, as indicated by Thomas *et al.* (1). We therefore treated the nonstoichiometric samples $Li_{1-x}NiO_2$ at 180°C for 192 hr. The samples after the heat treatment showed monophasic properties for $0.8 \leq y \leq$

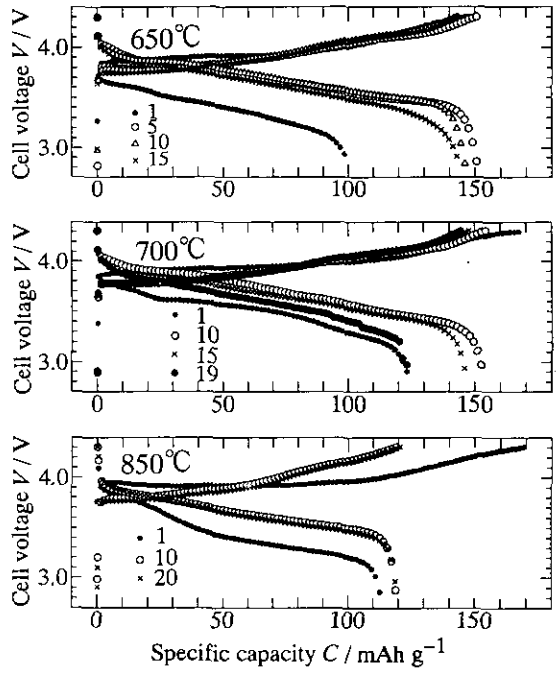

FIG. 7. Charge–discharge curves for the lithium cells using $LiNiO_2$ cathodes synthesized at 650, 700, and 850°C. The current density was 0.75 mA/cm^2.

1.8 in $Li_yNi_2O_4$; even the starting $Li_{1-x}NiO_2$ was a mixture of two rhombohedral (hexagonal) phases. Figure 8b shows the lattice parameter change with composition x in $Li_{1-x}NiO_2$ (the α-$NaFeO_2$ structure) or y in $Li_yNi_2O_4$ (the spinel structure). The cubic and rhombohedral(hexagonal) structures were observed for $0.8 \leq y \leq 1.1$ and $1.1 < y \leq 1.8$, respectively. These rhombohedral cells are different from those of the deintercalated $Li_{1-x}NiO_2$, indicating an intermediate type of cation distribution between the spinel and the α-$NaFeO_2$ structures.

Electrochemical Characteristics

The intercalation of $LiNi_2O_4$ spinel was examined using the cell $Li/Li_{1+x}Ni_2O_4$. Figure 9 shows discharge–charge curves together with the quasi-OCV curve for $Li_yNi_2O_4$ with $1.0 \leq y \leq 2.0$. On discharge, the cell voltage decreased rapidly to 1.80 V, and then decreased slightly to 1.75 V. This cell was charged again to the initial y value of 1.0. The X-ray diffraction pattern of the sample after the first discharge–charge cycle was the same as that of the initial one. Further, the quasi-OCV curve showed a gradual decrease in voltage from 3.0 V at $y = 1.0$ to 2.0 V at $y = 2.0$. These results indicate that the intercalation and deintercalation proceeded reversibly between $y = 1.0$ and 2.0 by a monophasic reaction. The nominal composition at $y = 2.0$ is "$Li_2Ni_2O_4$," which is the same composition as $LiNiO_2$. The X-ray diffraction pattern of $Li_2Ni_2O_4$ was indexed by the cubic cell with $a = 8.207(3)$ Å, which is larger than the lattice parameter $a = 8.087(2)$ Å for the $LiNi_2O_4$ spinel. The electrochemical intercalation followed by the low-temperature heat treatment gave the new polymorphism of $LiNiO_2$.

Electrical Properties

Electrical resistivities were measured for the spinel $Li_yNi_2O_4$ by a dc four-probe method. Because the spinels are unstable above 300°C, which prevents the fabrication of sintered pellets, the samples for the resistivity measurements were pressed into a pellet form by a pressure of 3 GPa using a cubic anvil-type high-pressure apparatus. Figure 10 shows the temperature dependence of the resistivity for $Li_yNi_2O_4$. The resistivity values and the activa-

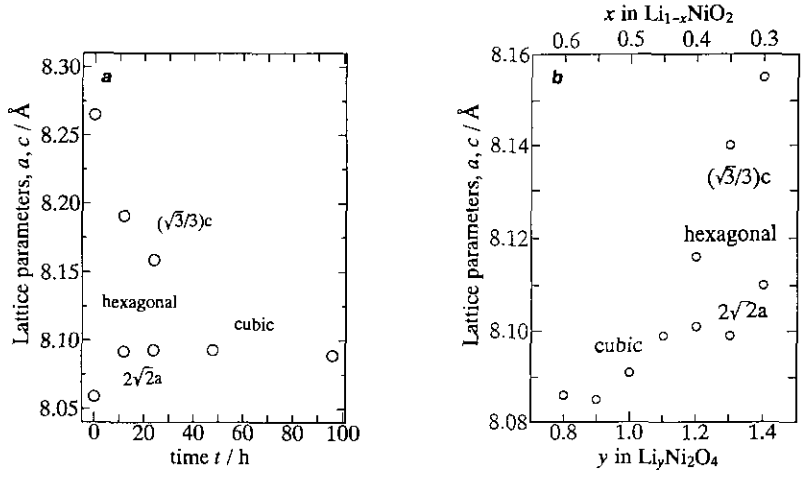

FIG. 8. (a) Annealing time dependence of lattice parameters for $Li_{0.5}NiO_2$. (b) Lattice parameters vs composition curves for $Li_yNi_2O_4$.

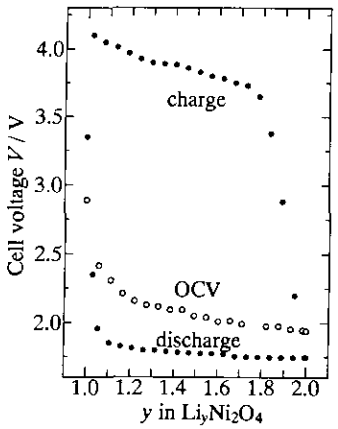

FIG. 9. Charge–discharge and quasi-OCV curves for $Li_yNi_2O_4$.

tion energies calculated near the room-temperature region are summarized in Table 4. The $Li_yNi_2O_4$ spinels show semiconducting properties with low activation energies. The resistivities and the activation energies decrease with decreasing y. The electrical property of the $LiNi_2O_4$ spinel has been reported to be semiconducting with the activation energy $E_a = 0.27$ eV (10), which is quite higher than those observed in the present study. The resistances measured with a compacted powder pellet might be affected by grain boundary resistivities, and the high pressure for the sample fabrication decreased the resistivity. The semiconductivity of our samples might also contain the grain boundary contribution, because the pellets were not sintered at higher temperatures; the low resistivity $Li_{0.9}Ni_2O_4$ might be very close to a metallic state when the grain boundary contribution is taken into account.

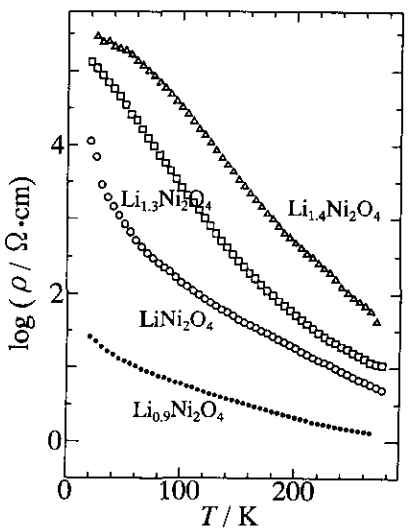

FIG. 10. Temperature dependence of the electrical resistivity for $Li_yNi_2O_4$.

TABLE 4
Electrical Properties for $Li_yNi_2O_4$

Composition y	Resistivity 265 K	ρ (Ω cm) 25 K	Activation energy E (eV)
0.9	1.4	23	0.01
1.0	5.9	7.1×10^3	0.03
1.3	12	1.1×10^5	0.04
1.4	59	2.9×10^5	0.08

SUMMARY

Phase Relationship between $LiNiO_2$ and its Related Compounds

$LiNiO_2$–NiO series. The phase relationship between $LiNiO_2$ and its related compounds is summarized. Only $LiNiO_2$–NiO solid solutions could be synthesized at elevated temperatures, as shown in Fig. 1. The stoichiometric $LiNiO_2$ is difficult to obtain; however, low-temperature synthesis has led to a compound fairly close to the stoichiometry. $LiNiO_2$ has a certain range of solid solution with a formula $Li_{1-x}Ni_{1+x}O_2$, as indicated by the previous studies (2, 4, 5, 9).

High-temperature treatment of $LiNiO_2$ caused a decomposition of $LiNiO_2$ to $Li_{1-x}Ni_{1+x}O_2$, which has a partially disordered cation distribution at the Li site. Further heating led to a complete decomposition to $Li_xNi_{1-x}O$ with random cation distribution at the octahedral site, followed by a two-phasic region with $Li_{1-x}Ni_{1+x}O_2$ and $Li_xNi_{1-x}O$. Higher oxygen partial pressure in the heat-treatment atmosphere suppressed the decomposition, which could be considered a reduction process from Ni^{3+} to Ni^{2+}.

Li_2NiO_2–$LiNiO_2$–NiO_2 series. Lithium intercalates into $LiNiO_2$ up to Li_2NiO_2, which has the tetragonal structure with space group $P3m1$, and has tetrahedral lithium and octahedral nickel ions in the hcp oxide ion packing (9). the deintercalation proceeded by a two-phasic reaction because of the anionic rearrangement from ccp to hcp array. This reaction is reversible (2).

The lithium deintercalation proceeds from $LiNiO_2$ to $Li_{0.3}NiO_2$ by a monophasic reaction when the cathode is mixed with Teflon binder and acetylene black. When the deintercalation was carried out using the cells with only $LiNiO_2$ cathodes, the deintercalation proceeded by subsequent monophasic and multiphasic reactions. Because of the relatively high lithium diffusion rate, the two-phasic region became smaller with the rest period after the electrochemical experiments. The monophasic regions of $0 \leq x \leq 0.05$, $0.3 \leq x \leq 0.35$, and $0.6 \leq x$ suggest the existence of vacancy ordering as indicated by Thomas *et al.* (1), which might be expressed by $Li_{1-x}NiO_x$, $Li_{2/3+x}NiO_2$, and

$Li_{1/3+x}NiO_2$, or they suggest the displacement of nickel ions from the Ni site to the Li site as indicated for $LiVO_2$ (22). However, no superlattice reflections were observed by the X-ray diffraction measurements.

$Li_{1-x}NiO_2$–$Li_yNi_2O_4$. The transformation from $Li_{1-x}NiO_2$ with the α-$NaFeO_2$ structure to the spinel $Li_yNi_2O_4$ proceeded below 300°C and was irreversible (1). This study revealed that the transformation proceeded in a wide range of compositions, $0 < x \leq 0.6$ in $Li_{1-x}NiO_2$. The spinel $LiNi_2O_4$ has two cation sites, the octahedral nickel site and the tetrahedral lithium site. The intermediate cation distribution between the α-$NaFeO_2$ and the spinel structures might be possible for the solid solution $Li_yNi_2O_4$.

Li_2NiO_2–$LiNi_2O_4$. Lithium intercalated into the cubic spinel $Li_yNi_2O_4$ from $y = 1.0$ to 2.0 and the reaction was reversible. The phase $Li_2Ni_2O_4$ obtained by the electrochemical intercalation has a cubic symmetry and is a new polymorphism of $LiNiO_2$.

REFERENCES

1. M. G. S. R. Thomas, W. I. F. David, J. B. Goodenough, and P. Groves, *Mater. Res. Bull.* **20,** 1137 (1985).
2. J. R. Dahn, U. von Sacken, and C. A. Michal, *Solid State Ionics* **44,** 87 (1990).
3. J. R. Dahn, U. von Sacken, M. W. Juzkow, and H. Al-Janaby, *J. Electrochem. Soc.* **138,** 2207 (1991).
4. J. Morales, C. Perez-Vicente, and J. L. Tirado, *Mater. Res. Bull.* **25,** 623 (1990).
5. W. Li, J. N. Reimers, and J. R. Dahn, *Phys. Rev. B* **46,** 3236 (1992).
6. T. Ohzuku, H. Komori, M. Nagayama, K. Sawai, and T. Hirai, *Chem. Express* **6,** 161 (1991).
7. J. P. Kemp, P. A. Cox, and J. W. Hodby, *J. Phys. Condens. Matter* **2,** 6699 (1990).
8. K. Hirota, H. Yoshizawa, and M. Ishikawa, *J. Phys. Condens. Matter* **4,** 6291 (1992).
9. I. Davidson, J. E. Greedan, U. von Sacken, C. A. Michal, and J. R. Dahn, *Solid State Ionics* **46,** 243 (1991).
10. G. Dutta, A. Manthiram, J. B. Goodenough, and J.-C. Grenier, *J. Solid State Chem.* **96,** 123 (1992).
11. J. N. Reimers, J. R. Dahn, J. E. Greedan, C. V. Stager, G. Liu, I. Davidson, and U. von Sacken, *J. Solid State Chem.* **102,** 542 (1993).
12. F. Izumi, "The Rietveld Method" (R. A. Young, Ed.), Chap. 13. Oxford Univ. Press, Oxford, 1993.
13. N. Watanabe, H. Asano, H. Iwasa, S. Satoh, H. Murata, K. Karahashi, S. Tomiyoshi, F. Izumi, and K. Inoue, *Jpn. J. Appl. Phys.* **26,** 1164 (1987).
14. Y. Takeda, R. Kanno, Y. Tsuji, and O. Yamamoto, *J. Electrochem. Soc.* **131,** 2006 (1984).
15. T. Sato, H. Ikeda, Y. Matsuda, and H. Tamura, *J. Appl. Electrochem.* **6,** 85 (1976).
16. Y. Matsuda, Y. Ouchi, and T. Tamura, *J. Appl. Electrochem.* **4,** 53 (1974).
17. H. N. Nigeon, A. Courtois, M. Zanne, and C. Gleitzer, *Rev. Chim. Miner.* **13,** 1 (1976).
18. W. R. Busing, K. O. Martin, and H. A. Levy, Report ORNL-TM-306. Oak Ridge National Laboratory, Oak Ridge, TN, 1964.
19. R. J. Gummow, M. M. Thackeray, W. I. F. David, and S. Hull, *Mater. Res. Bull.* **27,** 327 (1992).
20. R. J. Gummow and M. M. Thackeray, *Solid State Ionics* **53–56,** 681 (1992).
21. I. J. Pickering, J. T. Lewandowski, A. J. Jacobson, and J. A. Goldstone, *Solid State Ionics* **53–56,** 405 (1992).
22. J. G. Goodenough, G. Dutta, and A. Manthiram, *Phys. Rev. B* **43,** 10170 (1991).
23. M. M. Thackeray, L. A. de Picciotto, W. I. F. David, P. G. Bruce, and J. B. Goodenough, *J. Solid State Chem.* **67,** 285 (1987).